

A jet-induced outflow of warm gas in 3C 293

B.H.C.Emonts^{1*}, R.Morganti², C.N.Tadhunter³, T.A.Oosterloo²,
J.Holt³ and J.M.van der Hulst¹

¹*Kapteyn Astronomical Institute, University of Groningen, P.O. Box 800, 9700 AV Groningen, The Netherlands*

²*Netherlands Foundation for Research in Astronomy, Postbus 2, 7990 AA Dwingeloo, The Netherlands*

³*Department of Physics and Astronomy, University of Sheffield, Sheffield S3 7RH, UK*

ABSTRACT

Using long slit emission-line spectra we detect a fast outflow of ionized gas, with velocities up to 1000 km s^{-1} , in the nearby powerful radio galaxy 3C 293 ($z = 0.045$). The fast outflow is located about 1 kpc east of the nucleus, in a region of enhanced radio emission due to the presence of a distorted radio jet. We present results that indicate that this fast outflow is caused by a jet-ISM interaction. The kinematics of the outflowing ionized gas are very similar to those of a fast outflow of neutral hydrogen gas in this galaxy, suggesting that both outflows are the result of the same driving mechanism. While the mass of the outflowing ionized gas is about $1 \times 10^5 M_{\odot}$, the total HI mass involved in the neutral outflow is about $100 \times$ higher ($10^7 M_{\odot}$). This shows that, despite the high energies that must be involved in driving the outflow, most of the gas remains, or becomes again, neutral. Other outflows of ionized gas, although not as pronounced as in the region of the enhanced radio emission, are also seen in various other regions along the axis of the inner radio jets. The regular kinematics of the emission-line gas along the major axis of the host galaxy reveal a rotating ionized gas disk 30 kpc in extent.

Key words: galaxies: active - galaxies: individual: 3C 293 - galaxies: ISM - ISM: jets and outflows - ISM: kinematics and dynamics - line: profiles

1 INTRODUCTION

Nuclear activity can strongly influence the Interstellar Medium (ISM) in the centre of active galaxies. The strong radiation field from the central engine, as well as collimated jets of radio plasma, affect the ionization and kinematics of this ISM in a complex way. In addition, the situation can be further complicated by the presence of starburst-induced winds (e.g. Heckman, Armus & Miley 1990, and references therein), associated with young stellar populations that are known to be present in some radio galaxies (e.g. Aretxaga et al. 2001; Wills et al. 2002, 2004). The feedback mechanisms of AGN and starburst activity are also important in the evolution of the host galaxies. AGN activity may, for example, regulate the correlation between the mass of the central black hole and the galaxy's bulge properties (e.g. Silk & Rees 1998). It is therefore important to carefully study these physical processes and determine to what extent each of them influences the characteristics of the host galaxies. Nearby radio galaxies provide excellent opportunities to do this in detail.

An important feature that is observed in a signifi-

cant fraction of active galaxies is the presence of outflows of warm and hot gas from the central region (e.g. Heckman et al. 1981; Veilleux et al. 2002; Kriss 2004, and references therein). In a number of nearby powerful radio galaxies asymmetric emission-line profiles provide evidence for outflows of ionized gas, often with velocities $> 10^3 \text{ km s}^{-1}$ (e.g. Tadhunter 1991; Villar-Martin et al. 1999; Tadhunter et al. 2001; Holt, Tadhunter & Morganti 2003; Taylor, Tadhunter & Robinson 2003). Recently, a number of nearby radio galaxies have been found to contain such fast outflows not only in the ionized gas, but also in *neutral* hydrogen (HI) gas. Among these radio galaxies are 4C 12.50 (PKS 1345+12; Morganti et al. 2004a) and 3C 305 (Morganti et al. 2005). An overview of the HI outflows found so far in radio galaxies is given by Morganti, Oosterloo & Tadhunter (2004). The exact driving mechanisms for these fast outflows of neutral and ionized gas are not always clear, but they could consist of interactions between the ISM and the propagating radio plasma (like the case of Seyfert galaxy IC 5063; Oosterloo et al. 2000; Morganti et al. 2004b), AGN induced winds (e.g. Krolik & Begelman 1986; Balsara & Krolik 1993; Dopita et al. 2002) or starburst-related phenomena (e.g. Heckman, Armus & Miley 1990). The detection of neu-

* E-mail: emonts@astro.rug.nl

tral gas involved in the fast outflows puts serious constraints on the, most likely very energetic, driving mechanisms.

An excellent case to study the physical mechanisms in detail is the nearby powerful radio galaxy 3C 293, in which we recently detected an outflow of neutral hydrogen gas from the central region (Morganti et al. 2003, hereafter Paper 1). Velocities of the outflowing HI gas reach $\sim 1000 \text{ km s}^{-1}$, making it one of the most extreme cases of outflowing HI presently known. Unfortunately, due to limited spatial resolution of the observations we were not able to determine the exact location of this HI outflow. In this paper we analyse the characteristics of the ionized gas in 3C 293 and relate its kinematics with that of the outflowing neutral gas. We aim to gain a better understanding of the physical process that is responsible for the outflow and the effect it has on the ISM of the host galaxy.

3C 293 is a powerful ($P_{1.4\text{GHz}} \sim 2 \times 10^{25} \text{ W Hz}^{-1}$), edge-brightened Fanaroff-Riley type-II (Fanaroff & Riley 1974) radio source with two extended radio lobes (e.g. Bridle, Fomalont & Cornwell 1981, see also Figure 1). It also has a Steep Spectrum Core that consists of a true flat-spectrum radio core and a two-sided radio jet structure which is distorted and misaligned with respect to the outer radio lobes (e.g. Akujor et al. 1996; Beswick, Pedlar & Holway 2002, see also Figure 1). 3C 293 is hosted by the early type galaxy UGC 8782, that has a complex disk-like morphology with a bridge-tail structure that extends beyond a possible companion $\sim 33 \text{ arcsec}$ to the southwest (van Breugel et al. 1984; Heckman et al. 1986; Evans et al. 1999). The spectroscopic work of Tadhunter et al. (2005) reveals post-starburst young stellar populations with ages between 0.1 and 2.5 Gyr throughout the galaxy. 3C 293 has a modest far-IR luminosity of $L_{\text{fir}} \sim 2.3 \times 10^{10} L_{\odot}$. The galaxy contains extensive filamentary dust lanes (e.g. Martel et al. 1999) and large amounts of molecular and neutral hydrogen gas in the central few kpc (Baan & Haschick 1981; Haschick & Baan 1985; Evans et al. 1999; Beswick, Pedlar & Holway 2002; Beswick et al. 2004). Given its peculiar optical morphology and the presence of large amounts of cold gas and young stars, 3C 293 has often been suggested to have been involved in a gas-rich galaxy-galaxy interaction or merger event, in which large amounts of gas have been funnelled into the nuclear region and are now fuelling the AGN. The presence of a dense ISM, a young stellar population and a distorted radio morphology make 3C 293 an excellent case to study the interplay between ISM, nuclear starburst and AGN activity.

2 OBSERVATIONS

Optical long-slit spectra were taken at the William Herschel Telescope (WHT²) on May 12th 2001 (p.a. 60° and 135°) and in service mode on June 18th 2003 (p.a. 93°) using the ISIS long-slit spectrograph with the 6100\AA dichroic, the

¹ $H_0 = 71 \text{ km s}^{-1} \text{ Mpc}^{-1}$ used throughout this paper. At the redshift of 3C293, $z = 0.045$, this puts the galaxy at a distance of 190 Mpc and $1 \text{ arcsec} = 0.92 \text{ kpc}$.

² The WHT is operated on the island of La Palma by the Isaac Newton Group in the Spanish Observatorio del Roque de los Muchachos of the Instituto de Astrofísica de Canarias.

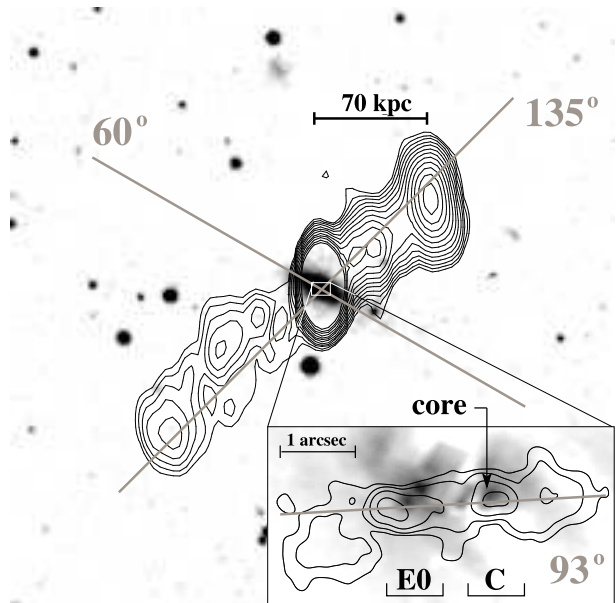


Figure 1. Position of the slits along 60° (major axis host galaxy), 135° (outer radio axis) and 93° (inner radio axis). The large-scale image is an overlay of WSRT radio contours (constructed from our 10 MHz data) superposed onto an optical DSS image of 3C 293. Contour levels in the WSRT image are 4.5, 6.5, 9.0, 13, 18, 25, 35, 50, 70, 95, 130, 170 mJy beam^{-1} . The zoom-in on the central region is an overlay of a MERLIN radio continuum image onto a HST F702W broadband image (overlay from Beswick, Pedlar & Holway 2002, see Section 3.1 for more details). Contour levels in the MERLIN image are 9, 36, 144, 630 mJy beam^{-1} . The regions C and E0 are the region of the core and the region of bright optical and radio emission 1 arcsec east of the core. These regions are described in detail in Section 3.1.

Table 1. Observational Parameters

date	p.a. ($^{\circ}$)	slit width ($''$)	integration time (s)		average airmass	seeing ($''$)
			blue	red		
5/12/2001	60	1.3	2400	2400	1.085	~ 0.8
5/12/2001	135	1.3	1200	1200	1.037	~ 0.8
6/18/2003	93	1.03	3600	2400	1.02	~ 1.0

R300B and R316R gratings at the blue and red arm and the GG495 blocking filter on the red arm to cut out second order blue light. This resulted in a wavelength coverage from about 3500 to 8000 \AA . The slit was aligned by eye and centred on the brightest part of the galaxy. The different slit positions are indicated in Figure 1. Table 1 gives a summary of the observational parameters.

We used the Image Reduction and Analysis Facility (IRAF) to reduce the data. A description of the data reduction of the May 12th 2001 data is already given by Tadhunter et al. (2005). For the June 18th 2003 data (p.a. 93°) the standard calibration (bias subtraction, flatfielding and wavelength calibration) was done. We used dome and arc exposures taken at approximately the same position and time as the source spectra. We took out a significant tilt of the slit in the spatial direction by applying a 1st order correction using two stars that were in the slit. With the tilt removed, the spectra are aligned within one pixel. Af-

ter the background subtraction the frames were combined and cosmic rays removed. Two standard stars (BD+26 2606 and BD+33 2642) were used for the flux calibration. The wavelength calibration was checked for both the 2003 and 2001 data using night skylines in spectra that were reduced without background subtraction. We corrected for any systematic off-set of the lines in the different spectra (likely due to flexure in the spectrograph) during the analysis of the spectra. The resulting accuracy of the wavelength calibration is within 0.1 \AA for all the red spectra and 0.4 \AA for all the blue spectra, with no obvious systematic errors. The λ -resolution of the spectra is $\sim 4 \text{ \AA}$.

For the analysis of the spectra, we used the Starlink package FIGARO to bin consecutive rows of pixels into a one-dimensional spectrum. In this way, we produced a series of spectra across the slit. These spectra were further analysed with the Starlink package DIPSO by fitting Gaussian profiles to the spectral lines. Velocities used in this paper are heliocentric velocities.

In order to study neutral hydrogen gas in emission around 3C 293 we obtained Westerbork Synthesis Radio Telescope (WSRT¹) observations on May 7th 2001, using the 10 MHz band. The goal of this study was to look for possible HI structures that could be reminiscent of a merger event in 3C 293. In the line data we detect three nearby companions of 3C 293 in HI emission, which we describe in detail in Emonts et al. (2004). However, as explained in Emonts et al. (2004), the bandwidth of these observations turned out to be not ideal for looking for HI emission directly associated with the host galaxy of 3C 293. In the present paper we use the WSRT data to make a new continuum image of 3C 293. The channels containing any deep HI absorption were excluded from the continuum fitting. We used the MIRIAD software to make the continuum image shown in Figure 1, which we use as a reference to show the slit alignments. The detection level of the radio continuum is limited by a dynamic range ~ 500 , while the peak intensity is 3.6 Jy beam^{-1} . The beam-size is $25.3 \times 11.9 \text{ arcsec}$ p.a. 1.1° . The total power is $P_{1.4\text{GHz}} \approx 2 \times 10^{25} \text{ W Hz}^{-1}$.

3 RESULTS

Extended continuum and emission-lines are detected in all our optical spectra of 3C 293. Figure 2 shows a typical spectrum of 3C 293 in the regions E0 and C (these regions are indicated in Figure 1 and will be described in detail below). In this Section various features of the emission-line gas in 3C 293 along the different slits are presented.

For the analysis of the kinematics of the gas we will mainly use the [SII] and [OII] lines. These are among the stronger emission lines detected and they do not suffer from absorption features in the underlying continuum as can be the case for the stronger $\text{H}\alpha$ line.

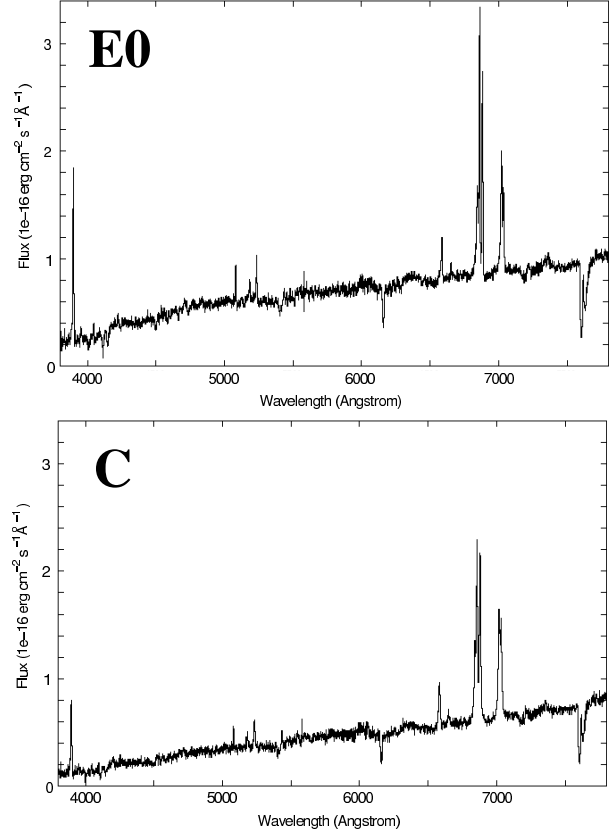


Figure 2. Spectrum of the regions E0 and C. The spectrum is a composite spectrum of both the red and the blue spectrum along p.a. 93° . The flux is summed over an aperture of 0.8 arcsec. See Section 3.3 for more details on these spectra.

3.1 Gas kinematics along the inner radio axis

In this section we concentrate on the analysis of the kinematics of the gas along the inner radio axis, i.e. p.a. 93° . Along this position angle the ionized gas clearly shows the most complex kinematics. This is illustrated by the 2D spectrum of the $\text{H}\alpha + [\text{N II}]\lambda\lambda 6548, 6583$ region shown in Figure 3. In this figure, the locations of the various features detected in the optical spectrum are compared with features seen in the radio and the HST image. Figure 3 (bottom) shows a MERLIN radio contour map overlaid on an optical HST image of the inner 5 kpc of 3C 293 (figure from Beswick, Pedlar & Holoway 2002, also shown in Figure 1). The accuracy of the overlay is within 0.3 arcsec. The HST WFPC2 image was taken with a broadband F702W filter and includes continuum in the wavelength range just below the strong $\text{H}\alpha + [\text{N II}]$ lines. In Figure 3 (middle) an integrated brightness profile from the HST image is taken across the region that is covered by the 93° slit, as indicated by the dotted region in the HST image. Figure 3 (top) shows that the different features in the HST image can be identified in the red part of our 2D-spectrum along p.a. 93° . Several regions of interest are indicated. Region C, when observed in the radio at VLBI resolution (Beswick et al. 2004), includes the actual core as well as a radio knot about 0.4 arcsec west of the nucleus. Region E0 is the region of peak intensity in the optical, about 1 arcsec east of the nucleus. This is also

¹ The WSRT is operated by the Netherlands Foundation for Research in Astronomy with support from the Netherlands Foundation for Scientific Research.

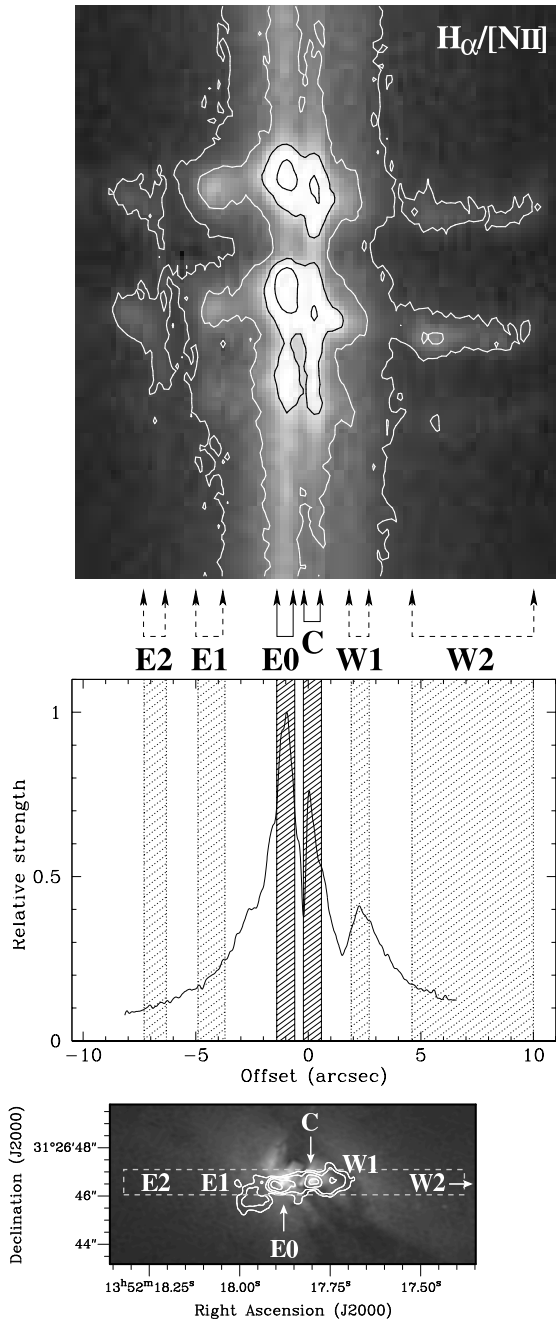


Figure 3. Bottom: MERLIN radio contour map overlaid on an optical HST image of the inner few kpc of 3C 293 (figure from Beswick, Pedlar & Holway 2002). Contour levels are 9, 36, 144, 630 mJy beam $^{-1}$. Middle: Integrated profile from the HST image across the region that is covered by the 93 $^{\circ}$ slit (indicated by the dotted region in the bottom plot). Top: Spectrum along p.a. 93 $^{\circ}$ ($H\alpha$ +[N II]). Contour levels: 0.75, 1.67, 3.4, 6.1 $\times 10^{-17}$ erg cm $^{-2}$ s $^{-1}$ Å $^{-1}$. The features in the spectrum can be traced in the HST image.

the region in which the radio continuum peaks. Regions E1 and W1 are regions east and west of the nucleus just at the edge of where fainter radio continuum is detected. Further out to the east and west (in regions where so far no radio continuum has been detected) are the regions E2 and W2.

In Figure 4 we show the 2D-spectrum of the [S II] dou-

plet. Also shown in Figure 4 are fits to the [S II] line at various places along the slit. As mention above, the [S II] line is used for the kinematic analysis in order to avoid possible effects of absorption features that may affect the H α line. Moreover, the region of the nucleus is more clearly seen in the red part of the spectrum than in the blue part (due to the higher sensitivity of the ISIS spectrograph in the red as well as complex extinction across the spectral range due to prominent central dust-lanes; Martel et al. 1999), which favours the use of [S II] above [O II] for the detailed kinematic analysis presented in this Section.

In Figure 4 we can immediately identify a narrow component in most of the fits. To fit the narrow component of the [S II] doublet we use two Gaussians with equal width and with wavelength separation constrained, following the physical parameters (corrected for the redshift of 3C 293) given by Osterbrock (1989). At most places along the slit we need a second, broader component to get a good fit (again this is a doublet component with equal width and wavelength separation constrained). Figure 5 shows various results from the line-fitting of both components of the [S II] line in the spectrum along 93 $^{\circ}$. Plotted against the distance of the features from the nucleus are the velocities of both the narrow and broad component relative to the systemic velocity of 3C 293, the velocity shift between the narrow and broad component, and the width of the broad component along the slit. Also shown is the line flux of both the narrow and broad components. Table 2 summarizes the kinematic information of both components in the different regions.

From Figures 4 and 5 and Table 2 we can distinguish several features with distinct gas kinematics. In Figure 5(a), the narrow components (connected with the dashed line) trace what appears to be a regular rotating feature that we identify with the large scale gas disk already observed by van Breugel et al. (1984). We will discuss more about this disk in Section 3.2. In the following we briefly discuss the characteristics of the ionized gas in each region:

- **Region C:** Region C is the region that includes the nucleus. In region C we need to include a broad component to get a good fit to the emission lines (Figure 4). This broad component, however, is strong compared to the broad component at other places along the slit and it peaks at the same velocity as the narrow component. It therefore might reflect a more turbulent state of the ionized gas close to the nucleus of the galaxy or the presence of a circum-nuclear disk. Similar phenomena have been suggested to to explain a broadening of the deep H I absorption profile in the nuclear region of 3C 293 (Beswick, Pedlar & Holway 2002).

At the location of the nucleus, we very accurately determine the systemic velocity of 3C 293 to be $v_{\text{sys}} = 13,450 \pm 35$ km s $^{-1}$ or $z = 0.04486 \pm 0.00012$, which is the redshift of the narrow component in region C. The error has been determined from the uncertainty in fitting the Gaussian components, from the inaccuracy of the wavelength calibration and from the uncertainty in the exact position of the nucleus in the optical spectrum.

- **Region E0:** Region E0 is the region about 1 kpc east of the nucleus, where both the optical as well as the radio continuum peak in intensity. In region E0 we detect, in addition to a narrow component, a broad component of the [S II] line that is highly *blueshifted* with respect to the velocity

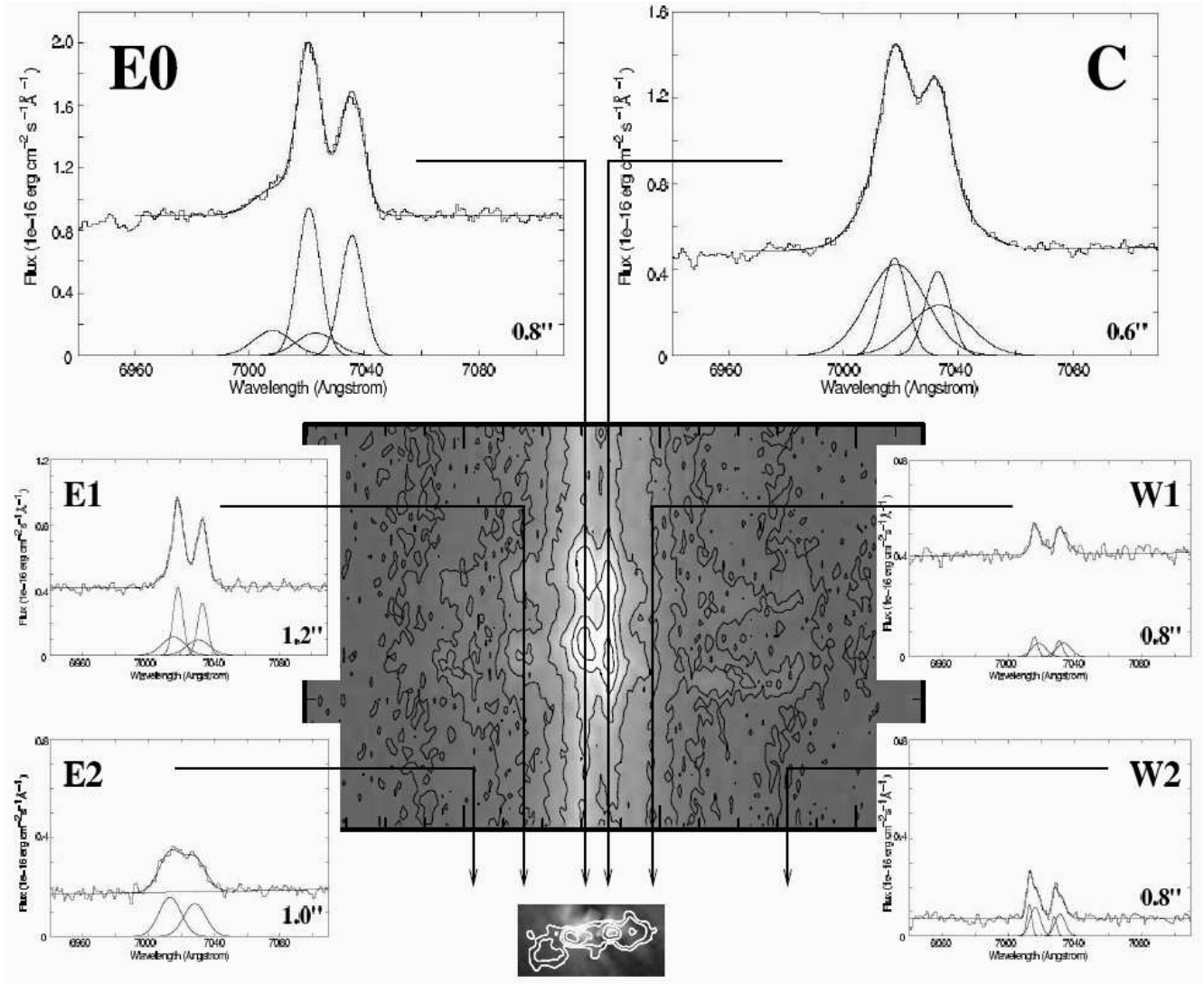


Figure 4. Spectrum of the [S II] $\lambda\lambda 6716,6731$ line (middle; contour levels 0.2, 0.48, 0.72, 1.1, 1.6, 2.5, 3.6, 4.6×10^{-17} erg cm $^{-2}$ s $^{-1}$ Å $^{-1}$). Also shown are the fits to the [S II] line at various places along the slit. At most places along the slit we need two components to get a good fit. The apertures used to make the 1D-spectra that we present here are written in the bottom-right corner of the plots (note that the plot of region W2 is taken with an aperture of 0.8 arcsec, but a similar spectrum is seen throughout the region W2 as it is indicated in Figure 3).

Table 2. Kinematic information of the various narrow and broad components observed in the different regions. Given is the FWHM (corrected for instrumental broadening) of the fit to both components as well as the velocity shift (Δv) between the centre of the broad component and the centre of the narrow component in each region (negative shift means that the broad component is blueshifted). Also given is the [S II] $\lambda\lambda 6716+\lambda 6731$ flux of the various components (given as the calculated mean flux over an aperture of 2 arcsec). Due to the faintness of the narrow component across region W2 we could not obtain a single good value for the width of this narrow component, therefore we left it out of this Table. Note that the broad component represents different gas features in the different regions (see text).

Region	FWHM $_{narrow}$ (km s $^{-1}$)	FWHM $_{broad}$ (km s $^{-1}$)	Δv (km s $^{-1}$)	Flux $_{narrow}$ ($\times 10^{-16}$ erg s $^{-1}$ cm $^{-2}$)	Flux $_{broad}$ ($\times 10^{-16}$ erg s $^{-1}$ cm $^{-2}$)
E2	-	664 ± 27	-202 ± 22	-	1.00 ± 0.04
E1	248 ± 15	687 ± 80	-114 ± 48	0.90 ± 0.10	0.61 ± 0.12
E0	341 ± 10	729 ± 127	-542 ± 56	4.02 ± 0.20	1.35 ± 0.26
C	411 ± 20	1032 ± 57	26 ± 31	3.12 ± 0.39	5.73 ± 0.64
W1	112 ± 55	398 ± 68	115 ± 75	0.19 ± 0.12	0.30 ± 0.12
W2	-	264 ± 40	152 ± 33	-	0.41 ± 0.09

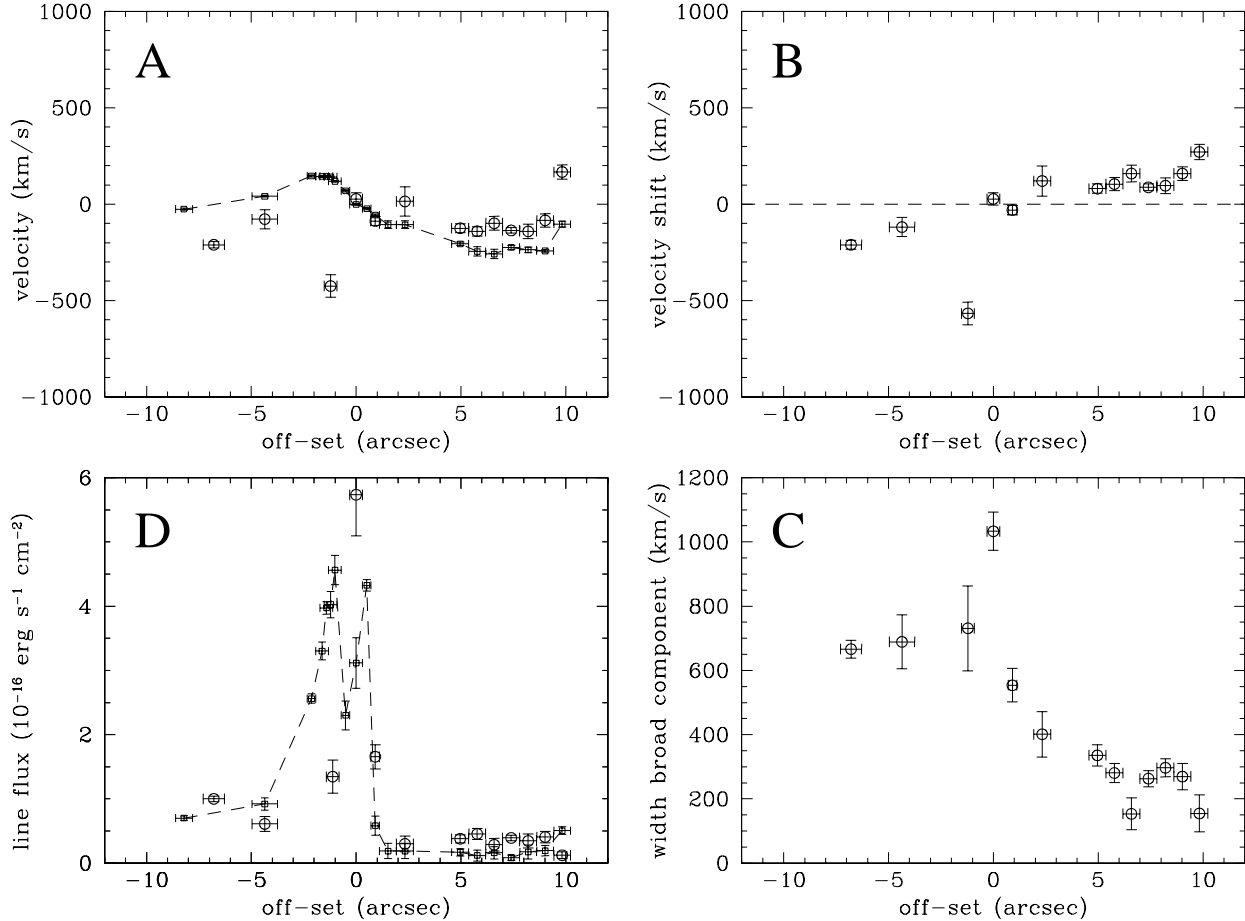


Figure 5. Line-fitting results of the [SII] line in the spectrum along 93° . In the various plots the small squares (connected with a dotted line) represent the narrow component of the gas. The circles represent the broad component. Vertical error bars represent uncertainties in the fits and in the λ -calibration; horizontal error bars represent the width of the used apertures. The horizontal axis is centred on the nucleus. Plotted against the spatial off-set from the nucleus are: (a) the velocity of both the narrow and the broad component w.r.t. the systemic velocity ($v_{\text{sys}} = 13,450 \pm 35 \text{ km s}^{-1}$; see Section 3.1); (b) the velocity shift between the broad and narrow component (the dotted line, velocity shift = 0, corresponds to the velocity of the narrow components); (c) the width of the broad component; (d) the [SII] $\lambda 6716 + \lambda 6731$ line flux (mean value over an aperture of 0.2 arcsec) of both the narrow and broad component.

of the narrow component and the systemic velocity of the system. A similar component is seen in the [OII] lines. The FWHM (full-width at half the maximum intensity) of this component is $729 \pm 127 \text{ km s}^{-1}$ (corrected for instrumental broadening) and its centre is blueshifted by $542 \pm 56 \text{ km s}^{-1}$ w.r.t. the velocity of the narrow component that traces the regular rotating gas disk (see Figure 5). The width of the broad component and the amplitude of the velocity shift (w.r.t the narrow component) are so large that they cannot be due to gravitational motions of the gas. Thus, we interpret this broad, blueshifted component as a fast outflow of ionized gas. The exact extent of this outflow - both along the radio jet as well as perpendicular to it - will be discussed in Section 4.1.

- **Region E1:** Region E1 is the region at the edge of the weak radio emission about 4 kpc east of the nucleus. In region E1 the [SII] emission line shows a broad component with $\text{FWHM} = 708 \pm 80 \text{ km s}^{-1}$. In this case, the centre of

this broad component is blueshifted by only $114 \pm 48 \text{ km s}^{-1}$ w.r.t. the narrow component. Thus, also this component may represent a gas outflow, although not as pronounced as in region E0.

- **Region E2:** A very remarkable feature can be seen in region E2 at ~ 7 arcsec east of the nucleus. In Figure 3 this feature clearly has a “comma”-like shape and the ionized gas disk seems distorted. This is strengthened by the fact that in region E2 we cannot identify the narrow component in the [SII] line. Instead, we fit a single broad component in region E2. The FWHM of this feature is $664 \pm 27 \text{ km s}^{-1}$. When extrapolating the velocity that the disk would have in region E2 (as traced by the narrow component in the regions adjacent to E2; see Figure 5-A), the centre of this broad component is blueshifted by $202 \pm 22 \text{ km s}^{-1}$, again indicating the presence of gas outflow also in this region. In region E2 there is no detection of radio continuum down to

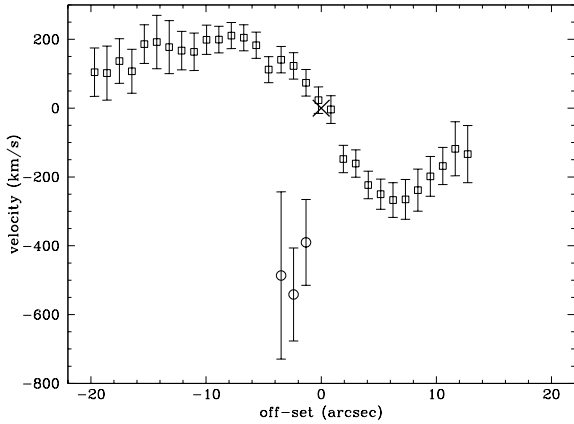


Figure 6. Position-velocity diagram of the [O II] line along the major axis of the galaxy (p.a. 60°). The squares trace the narrow component; the circles the broad component. Point (0,0) represents the nucleus. The off-set on the horizontal axis is the off-set (in arcsec) from the nucleus (error ± 0.6 arcsec). On the vertical axis the velocity is plotted w.r.t. the systemic velocity that we derive at the nucleus ($v_{\text{sys}} = 13,450 \pm 35 \text{ km s}^{-1}$; see Section 3.1). The vertical error bars represent uncertainties in the Gaussian fits and inaccuracies in the wavelength calibration.

a limit of 3 mJy beam^{-1} in radio continuum maps presented by e.g. Bridle, Fomalont & Cornwell (1981).

• **Regions W1 & W2:** Regions W1 and W2 are the regions west of the nucleus. In regions W1 and W2 the emission-line profile, although very faint, is clearly asymmetric. By including an additional, broader component we get an excellent fit to the emission-line profile in this part of the galaxy. The narrow component on the western side nicely traces the velocity curve of the gas disk, while the broader component is *redshifted* with respect to this narrow component. However, the FWHM of the fit to this broader component in regions W1 and W2 is only 398 ± 68 (W1) and 264 ± 40 (W2) km s^{-1} . Furthermore, the shift between the narrow and broad component is only 115 ± 75 (W1) and 152 ± 33 (W2) km s^{-1} . This redshifted component is not as pronounced as the blueshifted component seen on the eastern side of the galaxy. It might, therefore, indicate that only a mild outflow is present on the western side of the galaxy (with gas moving away from us). Another possibility is that this component might be caused by line-of-sight effects when we look through the almost edge-on disk of the galaxy. The asymmetric emission-line profile would then represent the narrow component gas at various locations in the disk, intercepted by our line-of-sight. With the data available to us we cannot disentangle these two possibilities.

The main result from this first part of the kinematic study of the ionized gas is that there are a number of locations along the position angle of the inner radio jet where gas outflows are observed. In addition to this, the most prominent outflow is observed at the location of the stronger radio continuum (E0). This will be further discussed in Section 4.

3.2 Extended gas disk

The spectrum taken along p.a. 60° follows the major axis of the galaxy. Therefore we also analysed the kinematics of the emission-line gas in this direction. Figure 6 show a velocity-curve of the ionized gas, constructed by fitting Gaussian profiles to the [O II] line, using apertures of 0.6 arcsec at various places along the 60° slit. Being one of the stronger lines, [O II] can be traced out to a larger distance from the centre than other lines. From this diagram it is clear that the [O II] emission-line gas follows the kinematics of a regular rotating disk (also seen by van Breugel et al. 1984). The plot also clearly shows how the blueshifted component observed in region E0 (the only one included in this slit position) is well separated from the gravitational motion of the regular rotating disk gas. The total diameter of the gas disk is 30 kpc, which is larger than the 19 kpc disk already found by van Breugel et al. (1984). A small difference in slit alignment might explain the slight deviation of our velocity curve from the one of van Breugel et al. (1984).

We centre the velocity curve on the systemic velocity that we derived in Section 3.1 ($v_{\text{sys}} = 13,450 \pm 35 \text{ km s}^{-1}$). Our value for v_{sys} is in agreement with $v_{\text{sys}} = 13,478 \text{ km s}^{-1}$, found with HI absorption at the core by Beswick et al. (2004). The redshift velocity of the disk gas in region E0 is roughly $13,500 \text{ km s}^{-1}$, consistent with the velocity of the deep, narrow HI absorption that is located against the enhanced radio emission in region E0 (Beswick, Pedlar & Holway 2002; Beswick et al. 2004) and with CO measurements (Evans et al. 1999). From our rotation curve along p.a. 60° we derive a velocity gradient of $\sim 57 \text{ km s}^{-1} \text{ arcsec}^{-1}$ in the inner region of the galaxy. This is consistent with the gradient seen by van Breugel et al. (1984) and with the gradient of $\sim 46 \text{ km s}^{-1} \text{ arcsec}^{-1}$ derived from HI absorption studies by Beswick, Pedlar & Holway (2002).

3.3 Ionization and density of the gas

Table 3 gives the values of the fluxes of the narrow component of various emission lines measured in the regions E0 and C in the spectrum along p.a. 93° (see Figure 2). The fluxes are the total emission-line fluxes, estimated from Gaussian fits, across an aperture of 0.8 arcsec (corresponding to a spatial binning of 4 consecutive pixels in the 2D-spectra) centred on regions E0 and C.

The line-ratios in Table 3 are not corrected for extinction. The ratio $\text{H}\alpha/\text{H}\beta = 9.5$ in region E0 is about a factor 3 too high when comparing it with the hydrogen recombination analysis done by Osterbrock (1989). Therefore it is clear that $\text{H}\beta$ is strongly affected by reddening (caused by various dust lanes that cross the inner region of 3C 293, e.g. Martel et al. 1999) and/or by underlying $\text{H}\beta$ absorption associated with the young stellar population that Tadhunter et al. (2005) found in this galaxy. Furthermore, the $\text{H}\alpha$ emission line could be affected by underlying atmospheric absorption. All this makes the analysis of the line ratios more complicated. Nevertheless, when comparing with diagnostic diagrams (e.g. Baldwin, Phillips & Terlevich 1981; Veilleux & Osterbrock 1987; Dopita & Sutherland 1995), we can use some of the

Table 3. Fluxes of the narrow component emission-line gas - relative to $H\beta$ - across an 0.8 arcsec aperture in regions E0 and C. The $H\beta$ flux is given in $\text{erg s}^{-1} \text{cm}^{-2}$. The errors are also scaled to the value of the $H\beta$ flux and reflect both the uncertainty of the Gaussian fits as well as the inaccuracy in determining the continuum level. Also included are the fluxes of the broad component of the [O II] and [S II] gas (scaled to the value of the narrow component) in region E0.

Element (narrow comp.)	Region E0 Flux relative to $H\beta$	Region C Flux relative to $H\beta$
$H\beta$ flux	$2.32 \pm 0.24 \times 10^{-16}$	$1.15 \pm 0.10 \times 10^{-16}$
[O II] λ 3727	4.2 ± 0.2	4.9 ± 0.1
[O III] λ 4363	< 0.3	-
[O III] λ 5007	1.2 ± 0.2	2.6 ± 0.1
[O I] λ 6300	1.2 ± 0.4	5.2 ± 0.1
$H\alpha$	9.5 ± 0.4	15.7 ± 0.7
[N II] λ 6583	7.7 ± 2.9	20.4 ± 3.8
[S II] λ 6716 + λ 6731	7.4 ± 0.3	21.9 ± 0.3
[O II] _{broad/narrow}	0.32 ± 0.05	-
[S II] _{broad/narrow}	0.30 ± 0.05	-

lines, which lie close together so that the line ratios are not affected by extinction too much (e.g. [N II]/ $H\alpha$, [S II]/ $H\alpha$ and [O I]/ $H\alpha$ ratios, together with [O III]/ $H\beta$), as good diagnostics for the classification. Using these diagnostics we can conclude that region E0 in 3C 293 has a LINER-type (Low Ionization Nuclear Emission-line Region) spectrum (Heckman 1980). Thus, the narrow component gas in region E0 is likely either shock ionized or photo-ionized by the AGN at low ionization parameter. The line ratios are inconsistent with photo-ionization by O and B stars (H II region) or by a strong power-law AGN component at high ionization parameter.

The [O II] and [S II] fluxes of the broad component gas associated with the outflow in region E0 are also listed in Table 3. We were not able to make an accurate fit of the broad component in region E0 to any other line than the strong [O II] and [S II] lines. Other lines also show evidence for a broad component, but due to the underlying continuum and the limited signal-to-noise (in combination with the complexity of some of the emission lines, like e.g. [N II]+ $H\alpha$) we were not able to get a reliable fit to these broad components.

The emission-line gas in region C (fitted with a single Gaussian component) appears to have ionization characteristics similar to the narrow line gas in region E0, although the measured $H\alpha/H\beta = 15.7$ indicates that region C is likely even more affected by dust-extinction than region E0. In region C the gas is also likely ionized either by shocks or by the AGN at low ionization parameter.

Electron densities of the gas can be derived from the [S II] λ 6716/ λ 6731 ratio (Osterbrock 1989). Figure 7 shows [S II] λ 6716/ λ 6731 for both the narrow and the broad component in the various regions along p.a. 93° (the fit is too uncertain across region W2 and therefore we leave it out of the plot). The broad component represents different features in the various regions (Section 3.1), which might be physically unrelated. Nevertheless, given the relatively large uncertainties, we do not see any difference in the [S II] ratio in the various regions. The weighted mean [S II] λ 6716/ λ 6731

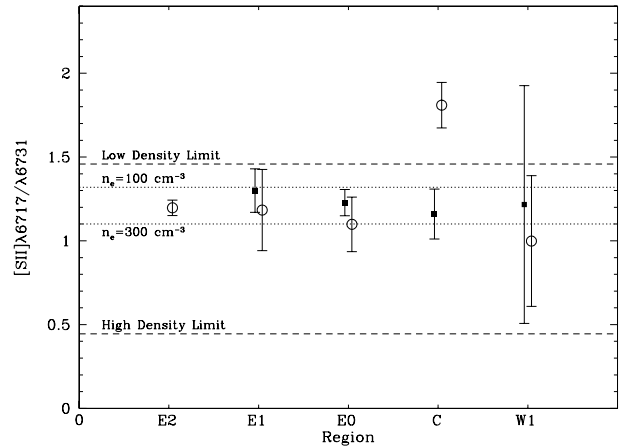


Figure 7. [S II] λ 6716/ λ 6731 of both the narrow emission-line gas component (open squares) as well as the broad emission-line gas component (open circles) in the various regions along p.a. 93° . Shown are the dotted lines that correspond to densities of 100 and 300 cm^{-3} (assuming $T = 10,000$ K, see Osterbrock 1989) as well as the maximum and minimum value for the [S II] doublet line ratio that is physically possible (the upper dashed line corresponds to $n_e \leq 10^4 \text{cm}^{-3}$, the lower dashed line to $n_e \geq 10^5 \text{cm}^{-3}$). The error bars reflect the uncertainty in fitting the Gaussian components.

ratio in Figure 7 is 1.23 ± 0.08 for the narrow component and 1.19 ± 0.07 for the broad component (excluding the broad component in region C, that does not represent an outflow; see Section 3.1). This corresponds to densities of about $2 \pm 1 \times 10^2 \text{cm}^{-3}$ for the narrow component and $3 \pm 1 \times 10^2 \text{cm}^{-3}$ for the broad component gas, assuming $T = 10,000$ K (since [O III] λ 4363 is not detected we are not able to derive the electron temperature of the emission-line gas). Thus, we do not see any significant difference between the density derived for the narrow and the broad component gas.

4 FAST GAS OUTFLOW IN REGION E0

The fastest outflow of gas is seen in region E0. In this region the emission lines are particularly strong and they allow some further analysis of the characteristics of this outflow. In particular we investigate in this Section the spatial extent of the region showing the fast outflow and we estimate the mass of the outflowing gas. This information will be used later on for building a possible scenario about the origin of this outflow.

4.1 Spatial extent of the gas outflow in region E0

In Figure 8 we analyse the extent of the region in which we detect the fast outflow. We do this by tracing the broad, blueshifted component of the [O II] emission line along the different position angles (since the [O II] line is stronger than the [S II] line it provides a better indication for the presence of the broad component). The top plots show in contours the HST F702W image of the central few kpc of 3C 293. The radio continuum of the MERLIN map (from Beswick, Pedlar & Holway 2002) is plotted in grey-scale

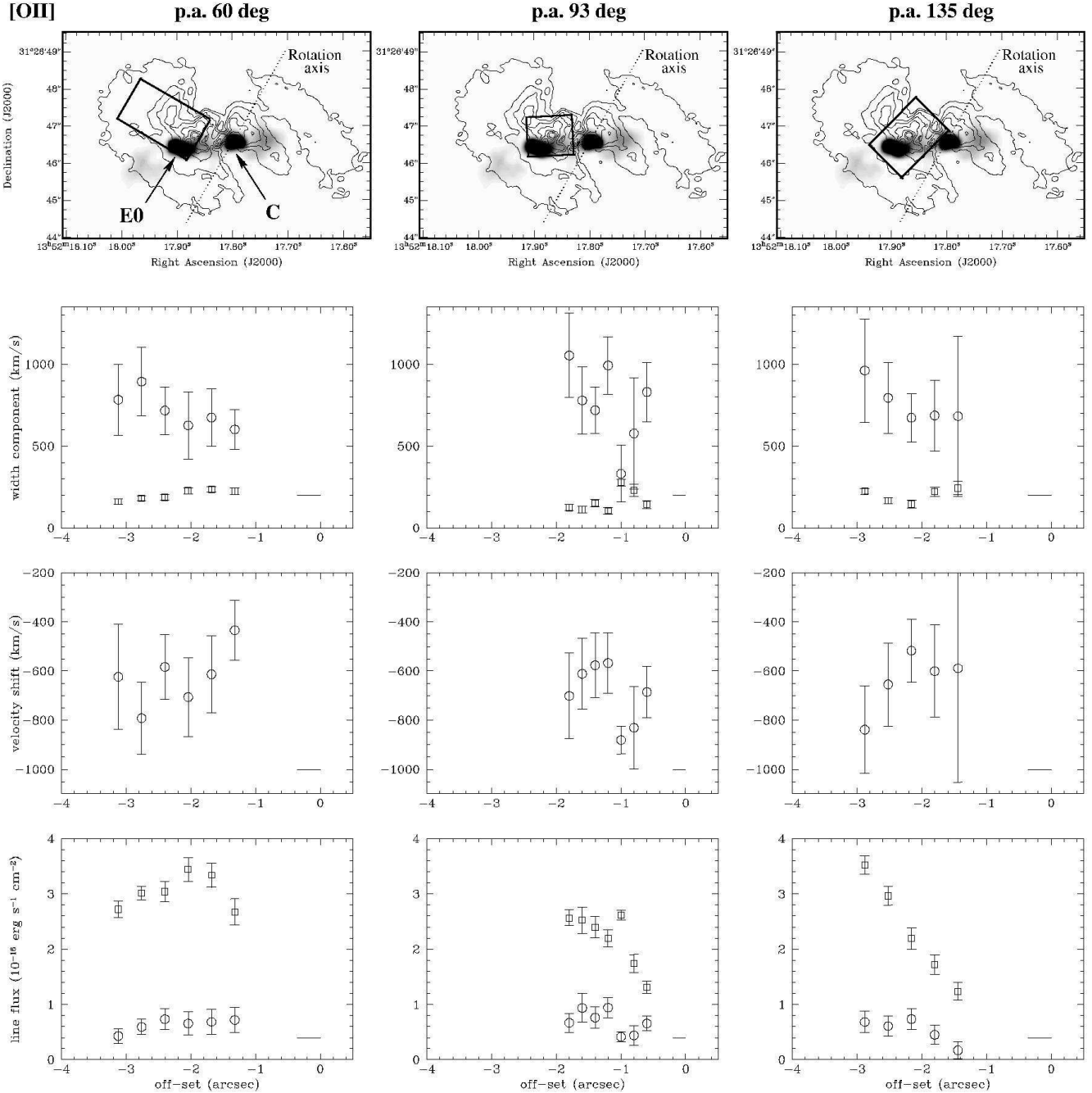


Figure 8. In the top plots contours of the HST F702W image of the inner region of 3C 293 are overlotted onto a grey-scale plot of the MERLIN radio continuum map. The dotted line presents the rotation axis of 3C 293 through the nucleus. The boxes indicate the region in which the broad, blueshifted component of the [O II] emission line is detected (see text for the accuracy of the position of the boxes). In the plots below that, various observed parameters are plotted. The first plot shows the width of the broad (circles) and the narrow (squares) component (corrected for instrumental broadening). The plots below that show the velocity shift between the broad and narrow component. The bottom plots show the line flux of both the broad (circles) and narrow (squares) component. The off-set on the horizontal axis is w.r.t. the nucleus, which we can determine with an uncertainty of 0.6 arcsec for the [O II] line. The horizontal bars in the bottom-right corner of the plots indicate the apertures over which we summed rows of pixels to extract the 1D-spectra (note that for the line flux along p.a. 60° and 135° we used a 0.4'' aperture and a 1.3'' slit width, while for the p.a. 93° the aperture was only 0.2'' and slit width 1.03'').

and clearly shows the knots of enhanced radio emission in the regions C and E0. The length of the boxes indicates the region in which the broad, blueshifted component is detected; the width of the boxes corresponds to the width of the slit. Note that the slit was aligned by eye to cover the brightest region and Figure 8 merely shows the most likely positioning of the slit. The uncertainty in the position of the nucleus in the spectra around the [O II] line (the “0”-point for the spatial off-set) is 0.6 arcsec. Also shown in Figure 8 are the width of the broad and narrow component, the velocity shift between the two components and the line flux of both components across the region in which the broad component is detected.

From Figure 8 and the seeing listed in Table 1 it is clear that the region in which the broad, blueshifted component is observed, i.e. the fast-outflow region, is spatially resolved. Not only is it resolved along the direction of the inner radio axis (where, moreover, we know already other regions of gas outflow do exist; see Section 3.1), but also perpendicular to it. The gas outflow is observed in a region of $2 \times 1.5 \text{ kpc}^2$.

4.2 Mass of the gas outflow in region E0

The mass of the gas in a line emitting region is related to the $H\beta$ luminosity in that region by:

$$M_{\text{gas}} = m_{\text{p}} \frac{L(H\beta)}{n_e \alpha_{H\beta}^{\text{eff}} h\nu_{H\beta}} \quad (1)$$

(see Osterbrock 1989), where n_e is the electron density (cm^{-3}), m_{p} the mass of a proton (kg), $L(H\beta)$ the $H\beta$ luminosity (erg s^{-1}), $\alpha_{H\beta}^{\text{eff}}$ the effective recombination coefficient for $H\beta$ ($\text{cm}^3 \text{ s}^{-1}$) and $h\nu_{H\beta}$ the energy of a $H\beta$ photon (erg). Assuming that the fast outflow is spread over an area of $2 \times 1.5 \text{ kpc}^2$ (Section 4.1) and accordingly over 1.5 kpc in our line-of-sight direction, we first estimate the luminosity of the narrow component gas of the disk in this outflow region to be $L(H\beta)_{\text{narrow}} = 1.3 \times 10^{40} \text{ erg s}^{-1}$. Here we assume that the extinction corrected flux (about $3\times$ the flux given in Table 3, which was measured with a slit aperture of $0.8 \times 1.03 \text{ arcsec}^2$; see Section 3.3), uniformly covers the region of outflow. This is a reasonable assumption, as can be seen from Figure 8 (bottom). To estimate the mass of the outflowing gas we need $L(H\beta)$ of the broad component gas. Unfortunately, the quality of the data did not allow us to unambiguously fit a broad component to the $H\beta$ line (see Section 3.3). Nevertheless, when assuming that the line ratio $H\beta_{\text{broad}}/H\beta_{\text{narrow}} \sim 0.3$ (similar to what we measured for [O II] and [S II]; Table 3), we derive for the $H\beta$ luminosity of the broad component $L(H\beta)_{\text{broad}} \approx 4.3 \times 10^{39} \text{ erg s}^{-1}$. Using the density derived in Section 3.3, we estimate that the *total mass of the outflowing ionized gas in region E0 is* $M \approx 1 \times 10^5 M_{\odot}$. The total ionized gas mass for the narrow component disk gas in the outflow region is $M \approx 6 \times 10^5 M_{\odot}$.

With the oversimplified assumption that the gas is locked up in clouds with a derived density of $3 \times 10^2 \text{ cm}^{-3}$ one can make an estimate for the filling factor (F_f) of these clouds over the region where we detect the fast outflow:

$$F_f = \frac{M}{nm_{\text{p}}V} \quad (2)$$

where M is the total mass of the outflowing gas, n the density of the gas, m_{p} the mass of a proton and V the volume of the region where the fast outflow is detected. Using the derived properties of the gas involved in the fast outflow, Equation 2 gives a filling factor of the outflowing gas of $F_f \approx 3 \times 10^{-6}$. Of course this is a rough estimate, since the distribution of the gas is unknown, but it is consistent with values derived in other powerful radio galaxies (van Breugel et al. 1985, 1986; Heckman et al. 1989; Koekemoer & Bicknell 1998). It shows that we are dealing with a clumpy medium in the central region of 3C 293.

5 COMPARISON WITH THE HI OUTFLOW

In Paper 1 we presented evidence for a fast outflow of neutral hydrogen gas in 3C 293. Figure 9 (from Paper 1) shows the broad but shallow HI absorption, mainly blueshifted w.r.t. the systemic velocity, that represents this fast outflow of HI. This absorption is detected against the central radio continuum using the 20 MHz band at the WSRT, but due to the low spatial resolution of the WSRT we are not able to locate the region in the inner radio structure from which the HI outflow originates.

In Emonts et al. (2004) we made a Gaussian fit to this broad HI absorption and derived a FWHM of $852 \pm 41 \text{ km s}^{-1}$. The centre of this Gaussian fit is $345 \pm 24 \text{ km s}^{-1}$ blueshifted from the deepest, narrow HI absorption feature, which traces quiescent gas likely located in an extended HI disk (Haschick & Baan 1985; Beswick, Pedlar & Holoway 2002; Beswick et al. 2004). The characteristics of the broad, blueshifted HI component look similar to those of the broad component of the ionized gas observed in region E0. A comparison between the two is shown in Figure 10 (from Paper 1). Region E0 therefore appears to be the most likely location for the fast HI outflow. The fact that the radio continuum is strongest in region E0 further strengthens this conclusion. The observed outflow of HI cannot be associated with the outflow of ionized gas that we see in region E2, since no strong radio continuum is detected in region E2. Moreover, at the resolution of the WSRT observations, the outflow would appear not coincident with the nucleus but displaced with respect to it.

The similarity between the characteristics of the HI outflow and the ionized gas outflow in region E0 suggests that they likely originate from the same driving mechanism.

If the broad component of the HI absorption is indeed located against the region E0, we can derive a new value for the HI column density. The peak intensity of the bright radio emission in region E0 in the MERLIN map of Figure 1 is 1.29 Jy. Therefore, the optical depth that the broad HI absorption feature has if it is located in region E0 is $\tau = 0.38\%$. This corresponds to column densities of the outflowing HI gas of $\sim 6 \times 10^{20} \text{ cm}^{-2}$ assuming $T_{\text{spin}} = 100 \text{ K}$. This value for the column density likely represents a lower limit, as in the extreme conditions under which these fast outflows occur the T_{spin} is likely (much) higher (e.g. Bahcall & Ekers 1969; Maloney, Hollenbach & Tielens 1996).

Assuming that the outflowing HI gas extends over the same region as the fast outflow of ionized gas, the HI column in front of the radio plasma will extend over $\sim 0.75 \text{ kpc}$.

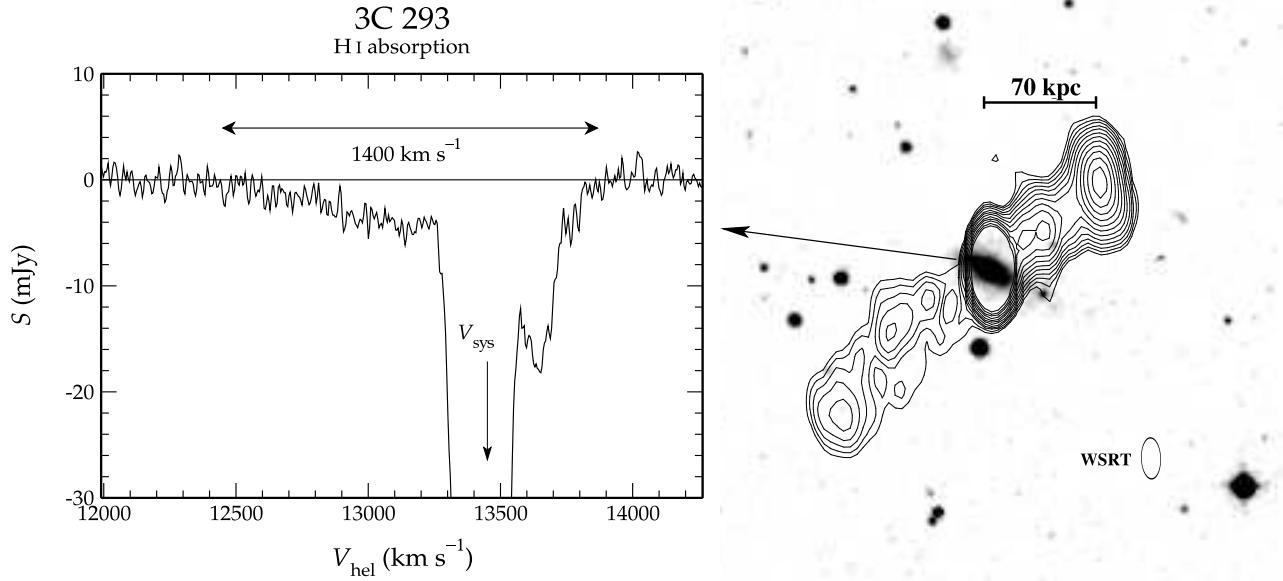


Figure 9. Right: Continuum image of 3C 293 made with our 10 MHz data. Left: Zoom-in on the HI absorption spectrum detected against the unresolved central radio continuum using the 20 Mhz band (Figure from Paper 1). Indicated is the full width at zero-intensity of the HI outflow.

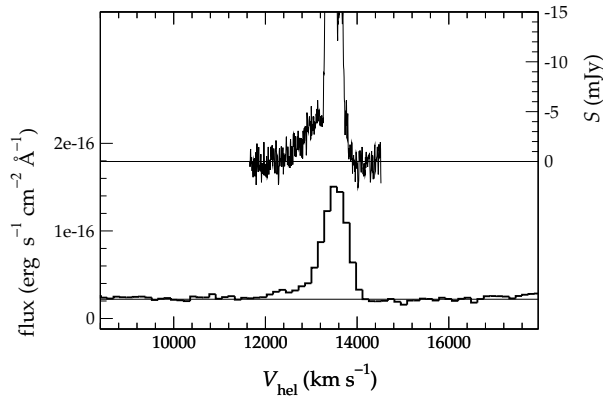


Figure 10. [O II] emission line in region E0 and HI absorption profile (inverted) plotted in one image.

The mean density of the neutral gas involved in the fast outflow will therefore be $\sim 0.3 \text{ cm}^{-3}$, which is comparable to the densities of $\sim 0.1 \text{ cm}^{-3}$ that Haschick & Baan (1985) found for HI clouds that are falling onto the AGN. However, given the very low filling factor that we derive for the ionized gas (Section 4.2), the neutral gas will most likely also be locked up in a clumpy medium with locally much higher densities. If the outflowing HI gas extends over the same region as the fast outflow of ionized gas in region E0 we derive a total HI mass of $M_{\text{HI}} \approx 10^7 M_{\odot}$ involved in the fast outflow. Although uncertainties are large (mainly due to the uncertainty in the exact location and extent of the HI outflow and due to the unknown spin temperature of the gas), the bulk of the outflowing gas nevertheless appears to be in a cold, neutral state and only a minor fraction is ionized.

6 DISCUSSION

The long slit spectra presented in this paper show complex kinematics of the ionized gas in the radio galaxy 3C 293, in particular along the position angle of the inner radio jets. At a number of locations we find outflows of ionized gas. The broader and most blueshifted gas-component, that we identify with a fast ($\sim 1000 \text{ km s}^{-1}$) outflow of ionized gas, is detected in the region E0, close to the brighter radio emission found along the jet. This is intriguing and suggests that the presence of the radio jet may play a role in producing the outflow. The total mass of warm gas involved in the fast outflow is $\sim 1 \times 10^5 M_{\odot}$. There are more regions in which complex kinematics of the ionized gas are seen, although less extreme than what we detect in region E0.

In addition to this, one of the most interesting results obtained is the similarity in the kinematic properties between the ionized gas outflow in the region E0 and the outflow of neutral hydrogen presented in Paper 1. *This suggest that the two outflows are coming from the same region (that would therefore be about 1 kpc from the nucleus) and that they are likely driven by the same mechanism.* The total HI mass of $10^7 M_{\odot}$ involved in the outflow shows that most of the outflowing gas is in its neutral state and that only a small fraction is ionized.

In the following, we will discuss some of the possible mechanisms that can cause such (off-nuclear) outflows, focusing in particular on the case of the region E0, for which detailed information could be derived from the optical data. Although the scenario of a jet-ISM interaction appears to be the most likely mechanism for the fast outflow in region E0, other mechanisms are also possible. We also briefly discuss what could be the cause for the milder outflows observed in other regions across 3C 293.

6.1 Driving mechanism for the fast gas outflow in region E0

Here we consider three possible mechanisms to explain the detected gas outflows, in particular the fast outflow detected in region E0.

- **Starburst driven wind:**

A possible driving mechanism for the outflow is acceleration of the gas by winds from young stars. By fitting the Spectral Energy Distribution (SED) at various places in 3C 293, Tadhunter et al. (2005) detected a young/intermediate age stellar population of 0.1 - 2.5 Gyr throughout 3C 293. Although starburst winds can generally produce outflows up to 1000 km s⁻¹, can easily carry enough energy for an outflow such as observed in 3C 293, and can predominantly shock-ionize the gas (e.g. Heckman, Armus & Miley 1990), it is not clear whether a starburst wind can survive over a period of 0.1 - 2.5 Gyr. Even if this is possible, a wind from this young/intermediate age stellar population would have to be “fossil” in order to still be visible at present. An outflow driven by such a fossil wind would no longer be localized to the region E0 where we see it, but would be many tens of kpc in extent.

It should be noted, however, that bright complexes of UV emission have been found throughout the disk of 3C 293 (Allen et al. 2002). Some of these complexes could contain young O and B stars, in which case winds from these young stars may contribute in some regions to the complex kinematics of the gas that we observe. The relatively poor accuracy of the astrometry between the UV image and the radio data does not allow us to reliably estimate how these complexes are located with respect to the radio features. It is worth noting, however, that one of the brighter UV complexes (one with an intriguing V-shaped morphology) could be located close to the region E0.

- **AGN radiation:**

Krolik & Begelman (1986) and Balsara & Krolik (1993) suggest that the continuum from the central engine can cause X-ray heated winds, which contain gas that evaporated off a surrounding torus. Their models show that the flow speeds of these winds can reach several hundred km s⁻¹ in the pc-scale region around the AGN. Following Dopita et al. (2002), also further from the nucleus the nuclear radiation can be responsible, if coupled to dust, for radiation pressure dominated gas outflows. This idea has been applied to the case of NGC 1068, where it can explain an outflow of ~ 700 km s⁻¹ at about 100 pc from the nucleus. A similar mechanism has been suggested in the case of Cygnus A (van Bemmel et al. 2003). In this case, the radiation from the powerful AGN in this radio galaxy can explain the outflow of ~ 170 km s⁻¹ observed in the ionization cone at about 1 kpc from the nucleus.

However, the AGN in the core of 3C 293 appears to be relatively weak compared with the objects considered above. Although obscuration certainly plays a role, we nevertheless find that the warm gas has a low ionization state in the centre of 3C 293. In particular, the [O III] λ 5007 line is weak. Alternatively, we can use the far-IR luminosity and assume that it is all due to re-radiated quasar-light instead of starlight. The far-IR luminosity of 3C 293, $L_{60\mu\text{m}}/L_{\odot} = 10.08$ (Golombek, Miley & Neugebauer

1988), is at the lower end of the luminosity for quasars (Neugebauer et al. 1986). This is more than an order of magnitude lower than for the nucleus of Cygnus A and about a factor 6 lower than for the nucleus of NGC 1068. It seems, therefore, unlikely that the radiation from the nucleus of 3C 293 is strong enough to accelerate the gas to the large velocities observed in region E0. Also in the case of Cygnus A, the much faster (~ 1800 km s⁻¹) outflow that has been detected along the radio axis in the [O III] emission lines (Tadhunter 1991) is not likely driven by AGN radiation pressure, but more likely explained as jet-induced.

- **Jet induced outflow:**

The fastest outflow of gas is seen ~ 1 kpc east of the nucleus in a region (E0) where there also is enhanced radio continuum due to a propagating radio jet. At VLBI-scale (e.g. Beswick et al. 2004) this radio jet shows a distorted morphology, including several bright knots, in particular near region E0. Beswick et al. (2004) argue that the radio jet in region E0 is approaching and that the continuum emission in this region might not be related to the fast jet itself, but rather to a low-velocity shear layer surrounding the jet, possibly created by an interaction between the jet and the ISM. In the central few kpc of 3C 293 there is a large reservoir of dense, cold gas, including HI clouds (with individual cloud masses \lesssim few times $10^6 M_{\odot}$; Haschick & Baan 1985; Beswick, Pedlar & Holoway 2002) as well as $1.5 \times 10^{10} M_{\odot}$ of H₂ (Evans et al. 1999). Overall these results suggest that the observed fast outflow of gas is caused by an interaction between the propagating radio jet and this dense ISM. Moreover, the outflow in 3C 293 resembles cases of jet-related outflows in other nearby powerful radio galaxies like Cygnus A (Tadhunter 1991), PKS 2250-41 (Villar-Martin et al. 1999), PKS 1549-79 (Tadhunter et al. 2001), PKS 1345+12 (Holt, Tadhunter & Morganti 2003) and 3C 305 (Morganti et al. 2005).

The total mass of warm gas involved in the outflow is $\sim 1 \times 10^5 M_{\odot}$, while the mass of the outflowing HI gas is $\sim 10^7 M_{\odot}$. We can estimate a mass outflow-rate of the gas, assuming that the outflow is free-floating and spherical in shape around the radio knot (we assume that the outflow covers at least 2π steradians as seen from the jet at the origin of the outflow):

$$\dot{M} \approx 2\pi R^2 \cdot \rho \cdot F_f \cdot v_{\text{out}} \cdot m_{\text{H}}, \quad (3)$$

with R the radius of the outflowing spheroid of gas, ρ the volume density and F_f the filling factor of this gas, v_{out} the velocity of the outflowing gas and m_{H} the mass of a H-atom. For the gas in region E0 that is flowing out at a velocity of 1000 km s⁻¹ in a spherical shell with radius $R = 0.75$ kpc we determine $\dot{M} \sim 0.1 M_{\odot} \text{ yr}^{-1}$ for the ionized gas and $\dot{M} \sim 23 M_{\odot} \text{ yr}^{-1}$ for the HI gas. Even if the inner radius of the spheroid of outflowing HI is not larger than the actual size of the radio knot ($r_{\text{knot}}=32$ pc; Akujor et al. 1996), the HI mass outflow-rate will still be of the order $1 M_{\odot} \text{ yr}^{-1}$. These outflow rates are conservative estimates, since the spin temperature of the outflowing gas is most likely higher than the assumed 100 K. The calculated outflow-rates are nevertheless in agreement with the total mass of the outflow that we see at present. In case of a steady-state outflow of gas, the outflow must have been driven for about the past 10^6 yr in order to get a total out-

flow of $M_{\text{HI}} \sim 10^7 M_{\odot}$ and $M_{\text{ion}} \sim 10^5 M_{\odot}$. During this time the outflowing gas has reached a distance of ~ 1 kpc, which is also in agreement with the size of the region in which we detect the outflow. Akujor et al. (1996) estimate the age of the outer radio structure to be $\sim 2.69 \times 10^6$ yr, assuming that the jet is moving freely at an advance speed of 0.1c. Their estimate of the age of the inner radio jets (when due to re-started activity) is $\sim 2.95 \times 10^4$ yr, although we note that there must be a large uncertainty in this estimate, given the fact that the inner radio jet is most likely relativistic (Beswick et al. 2004) and interacting with a dense ISM. Nevertheless, our best estimate of 10^6 yr for the age of the outflow implies that the radio plasma has been in interaction with the gas for a significant fraction of the total lifetime of the radio source. A total mass outflow-rate of $23 M_{\odot} \text{ yr}^{-1}$ is at the low end of galaxy-scale stellar winds observed by Rupke, Veilleux & Sanders (2002) in a sample of Ultra Luminous Infra-red Galaxies (ULIGs), indicating that the jet-ISM interaction could be an important factor in the evolution of this galaxy.

6.1.1 Details of the jet-ISM interaction

Let us now focus on how the gas is driven out by the radio jet, taking into account the energy-budget of the radio plasma. First we consider whether the radio power measured for 3C 293 is indeed sufficient to produce the observed outflow. The total power of 3C 293 is $P_{1.4\text{GHz}} \sim 2 \times 10^{25} \text{ W Hz}^{-1}$ (Section 2). Following Bicknell (2002) (and references therein), the rate at which radiating electrons are supplied to the radio lobes is proportional to the energy flux (F_E) of the radio plasma, so that:

$$\kappa_{\nu} = \frac{P_{\nu}}{F_E} \quad (4)$$

where $\kappa_{1.4\text{GHz}}$ is normally assumed or derived to be in the order of 10^{-12} - 10^{-11} for radio galaxies on the tens of kpc scale. Assuming $\kappa_{1.4\text{GHz}} = 10^{-12}$, and assuming that half of the energy flux is deposited in the eastern and the other half in the western jet/lobe structure, we expect that F_E is in the order of $10^{44} \text{ erg s}^{-1}$ for the eastern jet/lobe structure in 3C 293. From arguments mentioned in the previous Section, it is uncertain which part of the eastern radio jet/lobe structure is (and has been in the past) responsible for the fast outflow, and therefore also what the age of the outflow is. However, following the rough estimate from the previous Section that the outflow has been driven for about the past 10^6 yr, the total energy supplied by the radio jet in region E0 over this period is in the order of a few $\times 10^{57}$ erg. The total kinetic energy of the outflowing gas in region E0 is $E_{\text{kin}} = \frac{1}{2} M v^2 \approx 1 \times 10^{56}$ erg. We therefore argue that the radio plasma in 3C 293 carries enough energy to create the fast outflow in region E0.

The gas is accelerated by shocks that are created by the interaction between the jet and the surrounding medium. The gas outflow due to these shocks can be either momentum- or energy-driven. Let us first consider the momentum-driven case, in which the acceleration of the gas is caused by the impact of the working surface of the jet directly on a cloud. This happens when the jet is much lighter than the cloud. In this case only a small fraction of the jet energy flux is transmitted to the cloud, the rest is advected with the jet.

The momentum-flux (F_p) of a jet is only a small fraction of its energy-flux (Bicknell 2002):

$$F_p = \frac{1}{c} \times F_E \quad (\text{relativistic})$$

$$F_p = \frac{2}{v_{\text{jet}}} \times F_E \quad (\text{non-relativistic}), \quad (5)$$

For 3C 293 we saw that $F_E \approx 10^{44} \text{ erg s}^{-1}$ for the eastern jet/lobe structure. Beswick et al. (2004) argue that the inner radio jet is most likely relativistic, therefore $F_p \sim 3 \times 10^{33} \text{ g cm s}^{-2}$. We can also derive the total momentum-flux of the outflowing gas directly from our observations:

$$F_{p'} = \dot{M} \times v$$

$$\sim 6 \times 10^{34} \left(\frac{\dot{M}}{10 M_{\odot} \text{ yr}^{-1}} \right) \left(\frac{v}{1000 \text{ km s}^{-1}} \right) \text{ g cm s}^{-2} \quad (6)$$

Therefore we argue that it is unlikely that the outflow is entirely momentum-driven. However, given the uncertainty in the mass-outflow rate (Section 6.1), we cannot rule out this possibility.

Alternatively, (part of) the fast outflow in region E0 could be energy-driven by a jet-induced lobe expansion. In this scenario the gas is swept up and compressed as the radio jets hollow out a cocoon-like structure (e.g. Capetti et al. 1999; Tadhunter et al. 2001). According to Villar-Martin et al. (1999) outflow velocities $\gtrsim 1000 \text{ km s}^{-1}$ can more easily be explained if the clouds are entrained in hot, shocked gas that expands out behind the bow-shock, similar to the expansion of an interstellar bubble (see also e.g. Stone & Norman 1992; Dai & Woodward 1994; Klein, McKee & Colella 1994; O'Dea et al. 2003). This process has already been suggested for several other radio galaxies (e.g. Villar-Martin et al. 1999; Best, Röttgering & Longair 2000). Such a more gentle energy-driven mechanism might also be better for explaining the large amounts of neutral gas involved in the outflow.

6.1.2 Neutral gas involved in the outflow

The fact that only about 1 per cent of the outflowing gas appears to be ionized, while the rest is in its neutral state, is maybe one of the most intriguing results from this paper and Paper 1. The question is how, despite the high energies that must be involved in a jet-ISM interaction, such large amounts of gas stay, or become again, neutral?

The answer may lie within various simulations of jet-cloud interactions. For example, simulations by Sutherland, Bicknell & Dopita (2003) show that post-shock gas overtaken by a radio jet can show complex cooling. In the fractal structure of the gas dense filaments can be formed. Taking into account cooling effects, Saxton et al. (2005) and Bicknell, Saxton & Sutherland (2003) show that in various jet-ISM interactions intervening clouds can severely disrupt the radio jet, while at the same time some clouds are accelerated away from their initial positions by the thrust of the radio jet. Large clouds, in particular the ones not directly in the path of the jet, can survive for a long time after the radio jet passed. Simulations by Mellema, Kurk & Röttgering (2002) investigate the fate of a cloud of ionized gas that is overrun by the lobe of an expanding radio jet. Due to an underpressure in the cloud compared to the overpressured cocoon, shocks start

to travel into the cloud and the cloud is compressed and fragmented. Due to rapid cooling the bulk of gas gets locked up in these dense fragments that can survive for a long time and reach speeds up to 500 km s^{-1} . The further evolution of these fragments will be dominated by further acceleration and erosion by the passing flow, as well as gravitational collapse (which ultimately will result in star formation). Fragile et al. (2004) reach similar conclusions from their models on jet-induced star formation. They show that in the interaction of shocks with a radiative cloud, a large fraction of the cloud-gas cools to low temperatures. The neutral hydrogen gas in the starforming Minkowski's Object, for example, may have cooled from the initial warm gas as a result of the radiative cooling triggered by a passing radio jet. The amount of outflowing neutral hydrogen gas that we find in region E0 in 3C 293 might be explained in a similar way, although in the simulations by Fragile et al. (2004) the post-shock gas is only accelerated very slowly.

In light of the fast outflow of neutral hydrogen gas that we find in 3C 293, it would be interesting to explore whether, in the above mentioned simulations, at least a significant part of the dense clouds or fragments can consist of gas that remained or recombined again into neutral hydrogen gas, and if this gas can reach velocities up to 1000 km s^{-1} during the lifetime of the radio source.

6.2 Outflows in other regions

As explained in Section 3.1, there are other regions in which complex kinematics of the gas, possibly connected to outflows, are seen. However, the gas kinematics observed in the other regions are not as extreme as in region E0.

The propagating radio jet, responsible for the fast outflow in region E0 as explained above, likely carries enough energy to also cause outflows in the regions other than E0. This is an appealing scenario, in particular since the complex kinematics are observed along the inner radio axis. The fact that the broad component of the emission-line gas (the component that represents the ionized gas outflows) is blueshifted w.r.t. the narrow component on the eastern side and redshifted on the western side (in case the asymmetric emission-line profile in regions W1 and W2 represents a real outflow and is not the effect of observational line-of-sight effects as discussed in Section 3.1), implies that the radio jet is approaching on the eastern side and receding on the western side. However, in region E2 so far no radio continuum has been detected (see Section 3.1), although it is the region in between the bright inner radio jet and the bright outer radio lobe. This could mean that the radio jet is propagating more efficiently in this region and it might suffer from Doppler de-boosting. Something similar likely happens in the region between the core and the region E0 as observed with very high resolution VLBI imaging (Beswick et al. 2004). Another possibility is that the inner jet represent re-started activity (as suggested by Akujor et al. 1996), and the radio continuum in between the inner jet and the outer lobe has faded away. This last explanation could resemble the case of Centaurus A. As in 3C 293, also in Centaurus A a so called inner-filament of ionized gas with very complex kinematics (Morganti et al. 1991) is located outside the inner bright radio lobe (the lobe that can be considered to be the result of the most recent activity), but about 2 kpc from

the much fainter large-scale jet (Morganti et al. 1999). In the case of Centaurus A it has been proposed that the large velocities shown by the gas are still created by the strong instabilities produced by the propagation of the jet in the past (especially in the transition region between the inner and the outer lobe). A similar scenario could apply to the outflow observed in region E2 in 3C 293.

Using similar arguments to those used for region E0, the outflow in region E2, although it appears to have broken through the ionized disk of the galaxy, is still not spread widely enough that it can be explained by a fossil wind from the post-starburst stellar population found by Tadhunter et al. (2005). Also, from both our optical spectra as well as the UV-data from Allen et al. (2002), there is no indication that a substantially younger stellar population or H II region is present in region E2. Therefore it is not likely that the outflow in region E2 is driven by stellar winds.

An AGN-wind is not likely strong enough to explain the outflow in region E2, since the outflow seems to be too extreme for that. However, for the outflow in region E1 and in particular regions W1 and W2 (assuming the outflow is real in these western regions and not a result of observational line-of-sight effects as discussed in Section 3.1) we cannot discard an AGN-wind as the possible driving mechanism with the available data.

ACKNOWLEDGMENTS

We are grateful to T. Robinson for the reduction of the p.a. 60° and 135° spectra. BE would like to thank K. Wills for her help and advice, G. Bicknell and R. Sutherland for a very useful discussion and for giving good insights into jet-ISM interactions, and M. Villar-Martin for her tips on line-ratio analysis. We would also like to thank R. Beswick for providing his nice MERLIN-HST overlay and the support astronomers at the WHT for taking the high-quality spectra during service time. BE acknowledges the University of Sheffield and ASTRON for their hospitality during this project. Part of this research was funded by the Netherlands Organization for Scientific Research (NWO) under grant R 78-379.

REFERENCES

- Akujor C.E., Leahy J.P., Garrington S.T., Sanghera H., Spencer R.E., Schilizzi R.T. 1996, MNRAS, 278, 1
- Allen M.G. et al. 2002, ApJS, 139, 411
- Aretxaga I., Terlevich E., Terlevich R., Cotter G., Diaz, A.I. 2001, MNRAS, 325, 636
- Baan W.A., Haschick A.D. 1981, ApJ, 243, L143
- Balcall J.N., Ekers R.D. 1969, ApJ, 157, 1055
- Baldwin J.A., Phillips M.M., Terlevich R. 1981, PASP, 93, 5
- Balsara D.S., Krolik J.H. 1993, ApJ, 402, 109
- Best P.N., Röttgering H.J.A., Longair M.S. 2000, MNRAS, 311, 23
- Beswick R.J., Peck A.B., Taylor G.B., Giovanni G. 2004, MNRAS, 352, 49
- Beswick R.J., Pedlar A., Holloway A.J. 2002, MNRAS, 329, 620

- Bicknell G.V., Saxton C.J., Sutherland R.S. 2003, PASA, 20, 102
- Bicknell G.V. 2002, NewAR, 46, 365
- Bridle A.H., Fomalont E.B., Cornwell T.J. 1981, AJ, 86, 129
- Capetti A., Axon D.J., Macchetto F.D., Marconi A., Winge C. 1999, ApJ, 516, 187
- Dai W., Woodward P. 1994, ApJ, 436, 776
- Dopita M.A., Groves B.A., Sutherland R.S., Binette L., Cecil G. 2002, ApJ, 572, 753
- Dopita M.A., Sutherland R.S. 1995, ApJ, 455, 468
- Emonts B.H.C., Morganti R., Oosterloo T.A., Tadhunter C.N., van der Hulst J.M. 2004, to appear in "Extra-Planar Gas", ed. R. Braun, ASP Conf. Ser. Vol. 331, in press (astro-ph/0506391)
- Evans A.S., Sanders D.B., Surace J.A., Mazzarella J.M. 1999, ApJ, 511, 730
- Fanaroff B.L., Riley J.M. 1974, MNRAS, 167, 31
- Fragile P.C., Murray S D., Anninos P., van Breugel W. 2004, ApJ, 604, 74
- Golombek D., Miley G.K., Neugebauer G. 1988, AJ, 95, 26
- Haschick A.D., Baan W.A. 1985, ApJ, 289, 574
- Heckman T.M., Armus L., Miley G. 1990, ApJS, 74, 833
- Heckman T.M., Baum S.A., van Breugel W.J.M., McCarthy P. 1989, ApJ, 338, 48
- Heckman et al. 1986, ApJ, 311, 526
- Heckman T.M., Miley G.K., van Breugel W.J.M., Butcher H.R. 1981, ApJ, 247, 403
- Heckman T.M. 1980, A&A, 87, 152
- Holt J., Tadhunter C.N., Morganti R. 2003, MNRAS, 342, 227
- Klein R., McKee C., Colella P. 1994, ApJ, 420, 213
- Koekemoer A.M., Bicknell G.V. 1998, ApJ, 497, 662
- Krolik J.H., Begelman M.C. 1986, ApJ, 308, L55
- Kriss G.A. 2004, IAUS, 222, 223
- Maloney P.R., Hollenbach D.J., Tielens A.G.G.M. 1996, ApJ, 466, 561
- Martel A.R. et al. 1999, ApJS, 122, 81
- Mellema G., Kurk J.D., Röttgering H.J.A. 2002, A&A, 395, L13
- Morganti R., Oosterloo T.A., Tadhunter C.N., van Moorsel G., Emonts B. 2005, A&A, accepted, astro-ph/0505365
- Morganti R., Oosterloo T., Tadhunter C.N. 2004, to appear in "Extra-Planar Gas", ed. R. Braun, ASP Conf. Ser. Vol. 331, in press (astro-ph/0410222)
- Morganti R., Oosterloo T.A., Tadhunter C.N., Vermeulen R., Pihlström Y.M., van Moorsel G., Wills K.A. 2004a, A&A, 424, 119
- Morganti R., Oosterloo T.A., Emonts B.H.C., Tadhunter C.N., Holt J. 2004b, IAUS, 217, 332
- Morganti R., Oosterloo T.A., Emonts B.H.C., van der Hulst J.M., Tadhunter C.N. 2003, ApJ, 593, L69 (Paper 1)
- Morganti R., Killeen N.E.B., Ekers R.D., Oosterloo T.A. 1999, MNRAS, 307, 750
- Morganti R., Robinson A., Fosbury R.A.E., di Serego Alighieri S., Tadhunter C.N., Malin D.F. 1991, MNRAS, 249, 91
- Neugebauer G., Miley G.K., Soifer B.T., Clegg P.E. 1986, ApJ, 308, 815
- O'Dea C. P. et al. 2003, PASA, 20, 88
- Oosterloo T.A., Morganti R., Tzioumis A., Reynolds J., King E., McCulloch P., Tsvetanov Z. 2000, AJ, 119, 2085
- Osterbrock D.E. 1989, The Astrophysics of Gaseous Nebulae and Active Galactic Nuclei, University Science Books, Mill Valley, CA
- Rupke D.S., Veilleux S., Sanders D.B. 2002, ApJ, 570, 588
- Saxton J.S., Bicknell G.V., Sutherland R.S., Midgley S. 2005, MNRAS, 359, 781
- Silk J., Rees M.J. 1998, A&A, 331, L1
- Stone J.M., Norman M.L. 1992, ApJ, 390, L17
- Sutherland R.S., Bicknell G.V., Dopita M.A. 2003, ApJ, 591, 238
- Tadhunter C.N., Robinson T.G., González-Delgado R.M., Wills K., Morganti R. 2005, MNRAS, 356, 480.
- Tadhunter C., Wills K., Morganti R., Oosterloo T., Dickson R. 2001, MNRAS, 327, 227
- Tadhunter C.N. 1991, MNRAS, 251, 46
- Taylor M.D., Tadhunter C.N., Robinson T.G. 2003, MNRAS, 342, 995
- van Bemmell I.M., Vernet J., Fosbury R.A.E., Lamers H.J.G.L.M. 2003, MNRAS, 345, L13
- van Breugel W.J.M., Heckman T.M., Miley G.K., Filippenko A.V. 1986, ApJ, 311, 58
- van Breugel W.J.M., Miley G.K., Heckman T.M., Butcher H.R., Bridle A.H. 1985, ApJ, 290, 496
- van Breugel W., Heckman T., Butcher H., Miley G. 1984, ApJ 277, 82
- Veilleux S., Cecil G., Bland-Hawthorn J., Shopbell P.L. 2002, RMxAC, 13, 222
- Veilleux S., Osterbrock D.E. 1987, ApJ, 63, 295
- Villar-Martin M., Tadhunter C., Morganti R., Axon D., Koekemoer A. 1999, MNRAS, 307, 24
- Wills K.A., Morganti R., Tadhunter C.N., Robinson T.G., Villar-Martin M. 2004, MNRAS, 347, 771
- Wills K.A., Tadhunter C.N., Robinson T.G., Morganti R. 2002, MNRAS, 333, 211